ON THE USE OF NONLINEAR REGULARIZATION IN INVERSE METHODS FOR THE SOLAR TACHOCLINE PROFILE DETERMINATION

T. Corbard[1], G. Berthomieu[1], J. Provost[1] & L. Blanc-Féraud[2]

[1]Laboratoire Cassini, CNRS UMR 6529, OCA , BP 4229, 06304 Nice Cedex 4, France
[2]Projet Ariana, CNRS/INRIA/UNSA, 2004 route des Lucioles, BP 93, 06902 Sophia Antipolis Cedex, France

ABSTRACT

Inversions of rotational splittings have shown that the surface layers and the so-called solar tachocline at the base of the convection zone are regions in which high radial gradients of the rotation rate occur. The usual regularization methods tend to smooth out every high gradients in the solution and may not be appropriate for the study of a zone like the tachocline. In this paper we use nonlinear regularization methods that are developed for edge-preserving regularization in computed imaging (e.g. Blanc-Féraud et al. 1995) and we apply them in the helioseismic context of rotational inversions.

1. INTRODUCTION

The existence of high gradients in the solar rotation profile near the surface and at the base of the convection zone in the so-called *solar tachocline* (Spiegel & Zahn 1992) has been revealed by the inversions of the rotational splittings (see e.g. Thompson et al. (1996) and Schou et al. (1998) for the last results). The tachocline represents a thin zone where the differential rotation of the convection zone becomes rigid in the radiative interior. It is thought to be the place from where the solar dynamo originates and its precise structure is an important test for angular momentum transport theories. More precisely, the thickness of the tachocline can be related to the horizontal component of the turbulent viscosity and may be used as an important observational constraint on the properties of the turbulence (Spiegel & Zahn 1992; Gough & Sekii 1998; Elliot 1997).

Several works have already been performed to infer the fine structure of the tachocline (Charbonneau et al. 1998; Kosovichev 1996, 1998; Basu 1997; Corbard et al. 1998a; Antia et al. 1998) using both forward analysis and inverse techniques. For the inverse approach, it may be interesting to change the global constraint which tends to smooth out every high gradients in the solution and to find a way to preserve such zones in the inversion process. A first attempt in this direction has been carried out (Corbard et al. 1998a) by using a nonlinear regularization term through the PP-TSVD method (Hansen & Mosegaard 1996). An investigation of the possibility to use the elaborate nonlinear techniques, developed for edge-preserving regularization in computed imaging, in helioseismic context is being developed by Corbard et al. (1998b). Here we present preliminary results obtained by this method for the tachocline.

Section 2. briefly recalls the relation between the solar internal rotation and the helioseismic measured frequency splittings and presents the corresponding discretized inverse problem. We discuss in Section 3. the non linear approach of regularization in inverse techniques and the computational aspects. In Section 4., the choice of the regularizing parameters for the particular case of the solar rotation inversion and the preliminary results obtained with LOWL (Tomczyck et al. 1995, 2 years of data) and MDI (144 days, Schou et al. 1998) data are presented.

2. FORMULATION OF THE PROBLEM

In this paper we consider the 1D problem of inferring the solar equatorial rotation profile $\Omega_{eq} = \Omega(r, 90°)$ from sectoral splittings (i.e. $m = l$) (e.g. Duvall et al. 1984; Antia et al. 1996)

$$\frac{\nu_{nll} - \nu_{nl0}}{l} \simeq \int_0^{R_\odot} K_{nl}(r)\ \Omega_{eq}(r)\ dr, \qquad (1)$$

where l, n, m are respectively the degree, the radial order and the azimuthal order, r is the solar radius and $K_{nl}(r)$ are the so-called rotational kernels that have been calculated for each mode from a solar model taken from Morel et al. (1997).

This approximation of the 2D integral equation which relates the internal rotation to the splittings, is valid only for high degree modes (e.g. Corbard 1997) but the influence of low degree modes on the determination of the tachocline and upper layers is thought to be small. Moreover the rotation is known to be rigid or quasi rigid in the radiative interior.

We search a solution $\bar{\Omega}(r)$ as a piecewise linear func-

tion of the radius by setting:

$$\bar{\Omega}(r) = \sum_{p=1}^{N_p} \omega_p \psi_p(r) \quad \Omega \equiv (\omega_p)_{p=1,N_p} \tag{2}$$

where $\psi_p(r)$, $p = 1, N_p$ are piecewise straight lines ($N_p = 100$ in this work) between fixed break points distributed according to the density of turning points of modes (cf. Corbard et al. 1997). The discretization of Equation 1 leads to the matrix equation:

$$W = R\Omega, \tag{3}$$

where $W \equiv (W_i/\sigma_i)_{i=1,N}$ is the vector of the N observed frequency splittings W_i weighted by the standard deviation σ_i given by observers for each mode $i \equiv (n, l)$. No correlation between the different modes is assumed. The matrix R is defined by:

$$R \equiv (R_{ip})_{\substack{i=1,N \\ p=1,N_p}} \quad R_{ip} = \frac{1}{\sigma_i} \int_0^{R_\odot} K_i(r)\psi_p(r)dr \tag{4}$$

An inverse method should lead to a solution that is able to produce a good fit of the data. We define the goodness of the fit in chi-square sense by the χ^2 value obtained for any solution $\bar{\Omega}(r)$:

$$\chi^2(\bar{\Omega}(r)) = \sum_{nl} \left[\frac{W_i - \int_0^{R_\odot} K_i(r)\bar{\Omega}(r)dr}{\sigma_i} \right]^2, \tag{5}$$

which can be written in the discretized form:

$$\chi^2(\Omega) = \|R\Omega - W\|_2^2. \tag{6}$$

3. NON LINEAR REGULARIZATION

3.1. Euler equations

The inverse integral problem is an ill-posed problem and the minimization of only the χ^2 value generally leads to oscillatory solutions that are not 'physically acceptable'. So, a regularization technique must be used in the minimization process. A large class of these techniques can be expressed in the general form of the minimization of a criterion J over the unknown solution $\bar{\Omega}(r)$:

$$J(\bar{\Omega}(r)) = \chi^2(\bar{\Omega}(r)) + \lambda^2 \int_0^{R_\odot} \varphi\left(\left| \frac{d^q\bar{\Omega}(r)}{dr^q} \right| \right) dr, \tag{7}$$

The so-called trade-off parameter λ is chosen so that it establishes a balance between the goodness of the fit of the data and the constraint introduced on the solution (cf. Section 4.). The order q of the derivative is usually taken equal to one or two. The two choices can lead to similar results with the appropriate choice λ in the domains where the solution is well constrained by the data. In this work we consider only smoothing term with first derivative.

For a general φ-function, one can write the criterion Equation 7 in a discretized form:

$$J(\Omega) = \chi^2(\Omega) + \lambda^2 J_2(\Omega), \tag{8}$$

where $J_2(\Omega)$ represents the discretized regularization term defined by:

$$J_2(\Omega) = \int_0^{R_\odot} \varphi\left(\left| \frac{d\bar{\Omega}(r)}{dr} \right| \right) dr = \sum_{p=1}^{N_p-1} c_p \varphi\left(|L\Omega|_p \right). \tag{9}$$

In this equation $(c_p)_{p=1,N_p-1}$ represent the weights used for the integration rule, L is a discrete approximation of the first derivative operator, and $|L\Omega|_p$ is the absolute value of the p-component of the vector $L\Omega$. The expression of c_p and L are given in Corbard et al. (1998b) for the simple case of the polynomial expansion Equation 2

The minimization of the criterion $J(\Omega)$ leads to the following Euler equations (discretized form):

$$\nabla J(\Omega) = 0 \Longleftrightarrow (R^\top R + \lambda^2 L^\top B(\Omega) L)\Omega = R^\top W \tag{10}$$

B is a diagonal matrix. Its elements depend on the gradient of the solution at each grid point:

$$B = diag(b_p) \quad \text{with} \quad b_p = c_p \times \frac{\varphi'\left(|L\Omega|_p \right)}{2\,|L\Omega|_p} \tag{11}$$

Two choices for the φ-function lead to well known regularization strategies:

- $\varphi(t) = t^2$ corresponds to the traditional Tikhonov approach with first derivative whereas
- $\varphi(t) = t$ is known as the *Total Variation* (TV) regularization method (e.g. Acar & Vogel 1994). It has been shown that this regularization method is able to recover piecewise smooth solutions with steep gradients (Vogel & Oman 1996).

The use of a general nonquadratic φ-function will lead to a nonlinear problem which requires an appropriate iterative method to be solved.

3.2. Properties of the weight function $\frac{\varphi'(t)}{2t}$

From the Euler equation (Equations 10 and 11) we can see that the function $\varphi'(t)/2t$ acts as a weight function in the smoothing process: at each grid point the gradient of the solution is used as an argument of

this function in order to set locally more or less regularization. This suggests an iterative process where the gradient of the solution at a given step is used for the computation of the regularization term at the next step. Three properties of the weighting function $\varphi^{'}(t)/2t$ are required to obtain a satisfactory solution and to preserve high gradients (Charbonnier et al. 1997):

1. no smoothing for high gradients:

$$\lim_{t\to\infty} \frac{\varphi^{'}(t)}{2t} = 0 \tag{12}$$

2. Tikhonov smoothing for low gradients:

$$0 < \lim_{t\to 0} \frac{\varphi^{'}(t)}{2t} = M < \infty \tag{13}$$

3.

$$\frac{\varphi^{'}(t)}{2t} \quad \text{strictly decreasing to avoid instabilities.} \tag{14}$$

Either convex or non-convex φ-functions may be chosen (see Charbonnier et al. (1997) and Teboul et al. (1998) for examples in both cases). A non-convex function may be more suited for the search of high gradients. But this choice leads to some numerical difficulties and instabilities related to the existence of local minima and may induce a high sensibility of the inverse process to the regularization parameters. At the opposite the choice of a convex function avoids these numerical problems and is more suitable for relatively smooth transition (Blanc-Féraud et al. 1995).

3.3. The iterative algorithm: ARTUR

Following Charbonnier et al. (1997) the inversion using non linear regularizing criterion can be solved by an iterative scheme named ARTUR (Algebraic Reconstruction Technic Using Regularization) that is easy to implement: at each step k we calculate the regularization term using the derivative of the previous estimate Ω^{k-1} and we simply compute the new estimate Ω^k by solving the linear system:

$$\left(R^\top R + \lambda^2 L^\top B(\Omega^{k-1}) L\right)\Omega^k = R^\top W. \tag{15}$$

For a convex φ-function, the convergence of this so-called algorithm has been established (Charbonnier et al. 1997). This is therefore an adaptative regularization method which uses the information on the derivative of the solution obtained at each step in order to improve the regularization at the next step. This requires an initial guess Ω^0 for the solution but we will show in the next section that a constant solution can ever be used as the starting point.

An example of artificial discontinuous rotation has been used to test the algorithm. The corresponding rotational splittings have been computed according to Equation 1 with addition of Gaussian noise with a standard deviation taken for each mode from the formal error given in observational data (cf. Corbard et al. 1998a). A second set of artificial data with the same rotational law and standard deviations divided by $\sqrt{10}$ has also been used.

At each step of ARTUR algorithm the linear system (Equation 15) has been solved using an iterative conjugate gradient method using Ω^{k-1} as starting point. This leads to a very fast algorithm where the number of conjugate gradient iterations needed to solve the linear system decreases at each ARTUR step (i.e. as k increases). The algorithm is stopped when the norm of the relative difference between two solutions at two successive steps is below 10^{-6} i.e.:

$$\frac{\|\Omega^k - \Omega^{k-1}\|_2}{\|\Omega^k\|_2} \leq 10^{-6} \tag{16}$$

The results are given in Figures 1 and 2 which show examples of ARTUR steps (upper window). It is seen how the ARTUR solution, starting from a smoothed Tikhonov solution, becomes steeper at each step. Comparison between Figures 1 and 2 shows the effect of the errors in the data which leads to a smoothing of the edges of the discontinuity.

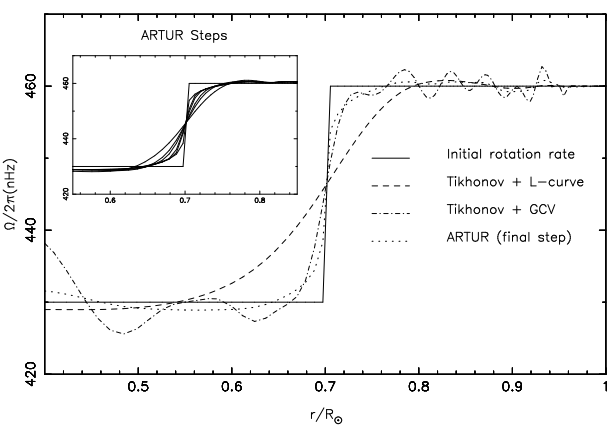

Figure 1. Solutions obtained by inverting splittings computed from a discontinuous one dimension rotation profile (full line) for the same mode set as in LOWL data and by adding some 'realistic' noise (see text). The standard Tikhonov solution is given for two different automatic choices of the regularizing parameter. The successive steps of ARTUR algorithm are given in the upper left window whereas the final step is shown on the main plot. The choice of the regularizing function and parameters for ARTUR algorithm are those discussed in Section 4. The solutions are plotted without error bars for clarity.

4. APPLICATION TO THE SOLAR ROTATION INVERSION

In the particular case of the solar tachocline, the uncertainty on the width of the transition zone is still large (see Table 2 of Corbard et al. (1998a) for a

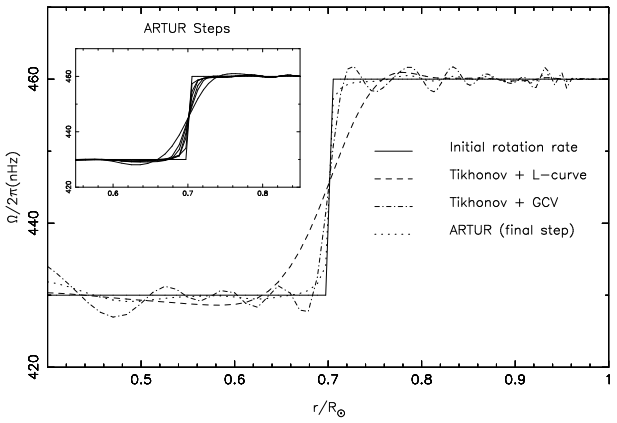

Figure 2. The same as Figure 1 but computed for a lower level of noise (standard deviations divided by $\sqrt{10}$). Comparison between Figures 1 and 2 shows the smoothing effect of the data noise level for the three methods.

summary of some previous works). Here we apply the non linear regularizing method to the LOWL and MDI sectoral splittings.

4.1. Choice of the φ-function

According to the previous discussion, we have chosen to consider a convex regularizing φ-function as Charbonnier et al. (1997):

$$\varphi(t) = 2\sqrt{t^2+1} - 2 \tag{17}$$

This function is close to the absolute value function used in TV regularization but has a quadratic behavior near 0 in order to smooth zones with small gradient moduli in addition to the linear behavior near infinity that preserves high gradient zones.

In addition to the usual regularizing parameter λ already introduced, we have included in the φ-function a parameter which scales the derivative of the solution. It allows to adapt the domain of gradient modulus where the solution is very weakly smoothed to the specific problem we consider.

$$J(\bar{\Omega}(r)) = \chi^2(\bar{\Omega}(r)) + \lambda^2 \int_0^{R_\odot} \varphi\left(\frac{1}{\delta}\left|\frac{d\bar{\Omega}(r)}{dr}\right|\right) dr \tag{18}$$

This simply leads to replace λ by $\overline{\lambda} = \lambda/\delta$ in Euler Equation 10 and to use

$$\varphi^{'}(t)/2t = 1/\sqrt{1+(t/\delta)^2} \tag{19}$$

where $t = |L\Omega|_p$ as weighting function in Equation 11.

Therefore we have to define a strategy to choose the two parameters $\overline{\lambda}$ and δ.

4.2. The choice of $\overline{\lambda}$

If the initial guess Ω^0 is a constant function, then, according to Equations 13 and 19, $M = 1$ and the solution at the first ARTUR step corresponds to a Tikhonov solution with $\overline{\lambda}$ as regularizing parameter. It has been shown in Corbard et al. (1998a) that the Generalized Cross Validation (GCV) strategy leads systematically to a less smoothed solution than the L-curve one (Hansen 1992) ($\lambda_{Lcurve} \simeq 100 * \lambda_{GCV}$ in that work) and therefore is more suited to the study of the tachocline. Nevertheless, this choice leads to spurious oscillations below and above the tachocline (see Figures 1, 2). As ARTUR algorithm will tend to enhance the high gradients found at the first step it is important to start with a solution smooth enough to avoid spurious oscillations with high gradients. At the opposite, the L-curve choice leads often to a solution which is too smooth and does not allow to exhibit the expected high gradients during the iterations. As the optimal choice of this parameter strongly depends on the level of noise included in the data (cf. Figures 1 and 2), it is important to define an automatic choice of this parameter so that we use the same strategy for different datasets or for different realizations of the noise. It consists in taking an intermediate value between the values of λ_{Lcurve} and λ_{GCV} for Tikhonov inversion. This has been used here to fix $\overline{\lambda}$ in ARTUR algorithm.

4.3. The choice of δ

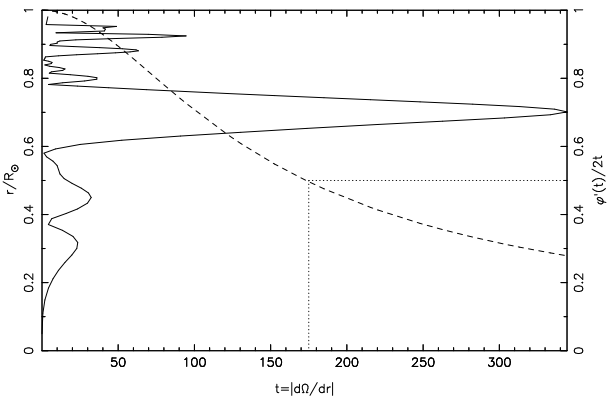

Figure 3. The full line shows the first derivative of a first step solution (cf. Figure 1) in ARTUR algorithm as a function of the fractional solar radius. For each value of the gradient, the dashed line gives the weight that will be given locally to the regularizing term at the second step of ARTUR algorithm. The dotted line indicates the gradient upon which the local regularization will be more than 50% smaller at the second step compared to the first step.

The parameter δ is introduced to adapt the shape of the weighting function to the gradient that we search to detect . Its value is chosen by looking at the derivative of the solution at the first iteration step. We have chosen for simplicity to keep this parameter constant during the iterations. Figure 3 shows as an example (full line) the first derivative of solution obtained at the first step by inverting artificial splittings which

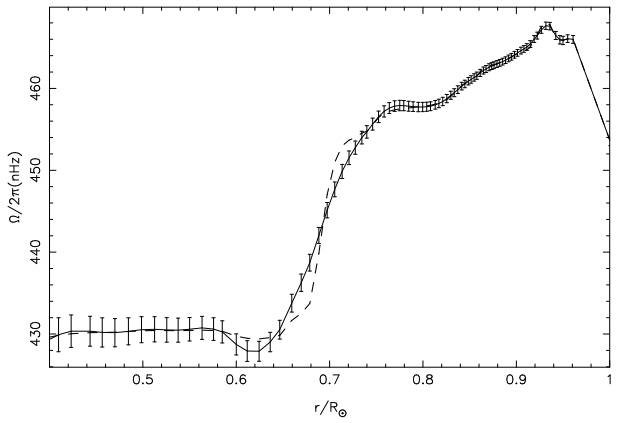

Figure 4. Solar equatorial rotation obtained by inverting LOWL data. Tikhonov solution is shown by the full line with error bars. The dashed line represents the final ARTUR step.

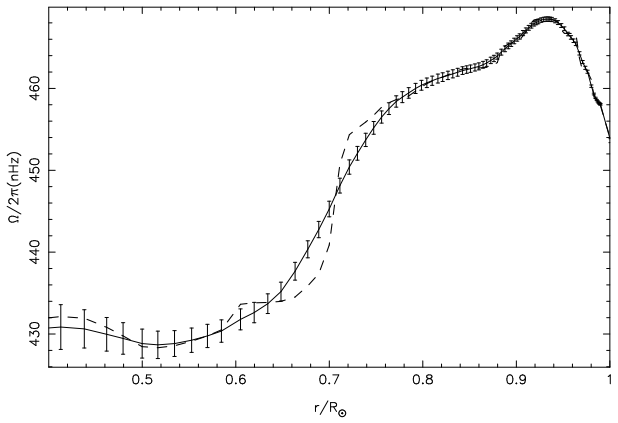

Figure 5. Same as Figure 5 for MDI data

have been computed for the discontinuous rotation law presented in the previous section (cf. Figure 1). The largest peak corresponds to the rapid variation in the tachocline, the smaller ones to spurious oscillations in the solution. The weighting function (Equation 19) is shown in dashed line for $\delta = 100$. According to Figure 3, the choice of $\delta = 100$ leads to regularize 50% less at the second step in that zones where the gradient of the first step solution is above ~ 175 nHz$/R_\odot$.

According to the previous results on solar rotation inversions, the width of the tachocline does not exceed 0.1 solar radius. This represents also the resolution reached at the tachocline localization ($\simeq 0.69R_\odot$) with a Tikhonov method using a regularizing parameter chosen near the corner of the L-curve. Furthermore we have a good estimate of the difference between the rotation rate above and below the transition ($\simeq$ 30nHz in Corbard et al. (1998a)). Therefore we can estimate an order of magnitude of 300nHz$/R_\odot$ for the maximum gradient obtained at the first iteration of ARTUR process. This corresponds to the value in Figure 3. At the second step we want to preserve only high gradients i.e. to regularize less in that zones where high gradients have already been found at the first step. With our a priori knowledge of the maximum gradient at the first step ($\sim$ 300nHz, see also Figure 3), the choice of $\delta = 100$ sounds reasonable in the sense that it will tend to decrease the regularization especially in the tachocline. A smaller value would enhance the secondary peaks that may be induced by the data noise.

4.3.1. Results for the tachocline

Figures 1 and 2 show that ARTUR algorithm leads always to better results than Tikhonov inversion without 'local deconvolution' in the case of a discontinuous rotation profile. Furthermore, it is shown in Corbard et al. (1998b) that it can also lead to good results for simulated tachocline widths between 0.02 and $0.08R_\odot$.

Preliminary results have been obtained by inverting the sectoral splittings given by the 2 years LOWL data and the 144 days MDI data. The results of Tikhonov inversion and the last step of ARTUR algorithm are plotted in Figures 4 and 5. Tikhonov solutions are shown with error bars at each grid points which are deduced from the propagation of data noise through this linear process. ARTUR algorithm is nonlinear and therefore we can not compute formal errors in the same way.

In order to have an estimate of the uncertainties on the tachocline parameters derived by ARTUR algorithm, Monte-Carlo simulations with artificial splittings have been performed by Corbard et al. (1998b). The rotation profiles were taken as erf functions with different 'initial widths'. Each 'inferred width' is the mean value of the results obtained by fitting directly the solutions by an erf function, for 500 realizations of input errors. Error bars are estimated from a 68.3% confidence interval. From this study it seems that an uncertainty of $\pm 0.02R_\odot$ on the tachocline width can be reached with both ARTUR algorithm and Tikhonov inversion with a 'local deconvolution' using the averaging kernels computed at the center of the transition (see Corbard et al. 1998b).

The width of the tachocline estimated from LOWL data and by using ARTUR algorithm is $0.05 \pm 0.02R_\odot$ in good agreement with the value of $0.05 \pm 0.03R_\odot$ found for the same data in Corbard et al. (1998a) by studying systematically the effect of regularization on the determination of tachocline parameters for three inverse methods. A preliminary study of MDI data leads to a slightly larger width of $0.08R_\odot$ but Monte-Carlo simulation have not yet been performed that allows to give an estimate of the uncertainty on this value. For both dataset the widths obtained from Tikhonov inversions after 'local deconvolution' using averaging kernels are always larger ($\sim 0.1R_\odot$) than the estimates obtained with ARTUR algorithm.

We note that these estimates of the tachocline width have been obtained by fitting the solutions by an erf function between 0.4 and $0.8R_\odot$ and this may be better adapted to the shape of LOWL solution (Figure 4) which presents a step between 0.75 and $0.8R_\odot$. This step is not found with MDI data and this may explain the larger width found by our fit with these

data. One possibility for future work is to change our fitting function i.e. to change our definition of the tachocline width. However we have also to explain the different behavior of the two solutions near $0.8R_\odot$ and to look if this remains with longer time series of MDI experiment.

ACKNOWLEDGMENTS

We acknowledge SOI team and S. Tomczyk for allowing the use of MDI and LOWL data. SoHO is a project of international cooperation between ESA and NASA. This work has been performed using the computing facilities provided by the program "Simulations Interactives et Visualisation en Astronomie et Mécanique" (SIVAM, OCA, Nice) and by the "Institut du Développement et des Ressources en Informatique Scientifique" (IDRIS, Orsay). T. Corbard thanks the conference organizers for financial support.

REFERENCES

Acar, R., Vogel, C.R. 1994, Inverse Problems 10(6), 1217

Antia, H.M., Basu, S., Chitre, S.M. 1998, MNRAS, submitted

Antia, H.M., Chitre, S.M., Thompson, M.J. 1996, A&A 308, 656

Basu, S. 1997, MNRAS 288, 572

Blanc-Féraud, L., Charbonnier, P., Aubert, G., Barlaud, M. 1995, In: IEEE Proceedings of the 2nd International Conference of Image Processing, Washington DC, USA, p. 474

Charbonneau, P., Christensen-Dalsgaard, J., Henning, R., et al. 1998, In: Provost J., Schmider F.X. (eds.) IAU Symp. 181: Sounding Solar and Stellar Interior (poster volume). OCA & UNSA, Nice, p. 161

Charbonnier, P., Blanc-Féraud, L., Aubert, G., Barlaud, M. 1997, IEEE Trans. on Image Processing 6(2), 298

Corbard, T. 1997, In: Proceedings of IX IRIS meeting, in press

Corbard, T., Berthomieu, G., Morel, P., et al. 1997, A&A 324, 298

Corbard, T., Berthomieu, G., Provost, J., Morel, P. 1998a, A&A 330, 1149

Corbard, T., Blanc-Féraud, L., Berthomieu, G., Provost, J. 1998b, A&A, to be submitted

Duvall Jr, T.L., Dziembowski, W.A., Goode, P.R., et al. 1984, Nature 310, 22

Elliot, J.R. 1997, A&A 327, 1222

Gough, D.O., Sekii, T. 1998, In: Provost J., Schmider F.X. (eds.) IAU Symp. 181: Sounding Solar and Stellar interior (poster volume). OCA & UNSA, Nice, p. 93

Gough, D.O., Thompson, M.J. 1991, The inverse problem. In: Cox A.N., Livingston W.C., Matthews M. (eds.) Solar Interior and Atmosphere. The University of Arizona Press, Tucson, p. 519

Hadamard, J. 1923, Lectures on the Cauchy Problem in linear Partial Differential Equation, Yale University Press, New Haven

Hansen, C.J., Cox, J.P., Van-Horn, H.M. 1977, ApJ 217, 151

Hansen, P.C. 1992, SIAM Review 34, 561

Hansen, P.C., Mosegaard K. 1996, Numerical Linear Algebra with Applications 3(6), 513

Hansen, P.C., Sekii, T., Sibahashi, H. 1992, SIAM J. Sci. Stat. Comput. 13, 1142

Kirsch, A. 1996, An Introduction to the Mathematical Theory of Inverse Problems, Springer-Verlag, New York

Kosovichev, A.G. 1996, ApJ 469, L61

Kosovichev, A.G. 1998, In: Provost J., Schmider F.X. (eds.) IAU Symp. 181: Sounding Solar and Stellar Interior (poster volume). OCA & UNSA, Nice, p. 97

Morel, P., Provost, J., Berthomieu, G. 1997, A&A 327, 349

Schou, J., et al. 1998, ApJ, submitted

Spiegel, E.A., Zahn, J.P. 1992, A&A 265, 106

Teboul, S., Blanc-Féraud, L., Aubert, G., Barlaud M. 1998, IEEE Trans. on Image Processing 7(3)

Thompson, M.J. et al. 1996, Science 272, 1300

Tikhonov, A.N. 1963, Sov. Maths. Doklady 4, 1035

Tomczyk, S., et al. 1995, Solar Phys. 159, 1

Vogel, C.R., Oman, M.E. 1996, SIAM Journal of Scientific Computing 17(1)